

# Cosmic ray $e^+e^-$ spectrum excess and peak feature observed by the DAMPE experiment from dark matter

Hong-Bo Jin,<sup>1,2</sup> Bin Yue\*,<sup>1,2</sup> Xin Zhang,<sup>1,2</sup> and Xuelei Chen<sup>†1,2,3</sup>

<sup>1</sup>*Key Laboratory of Computational Astrophysics, National Astronomical Observatories, Chinese Academy of Sciences, 20A Datun Road, Chaoyang District, Beijing, 100012, China*

<sup>2</sup>*School of Astronomy and Space Science, University of Chinese Academy of Sciences*

<sup>3</sup>*Center of High Energy Physics, Peking University, Beijing 100871, China*

(Dated: November 15, 2018)

The Chinese satellite Wukong, also known as the Dark Matter Particle Explorer (DAMPE) experiment, has released its observation data of the cosmic ray (CR) electrons and positrons. The data shows an excess in the energy spectrum up to TeV energy, and possibly also a peak-like fine structure at  $\sim 1.4$  TeV. We investigate the scenario that the source of the excess comes from the annihilation or decay of dark matter particles. We consider the  $W^+W^-$  channel and direct  $e^+e^-$  channel (model A), and the double  $\tau^+\tau^-$  channel and direct  $e^+e^-$  channel (model B). We find that the annihilation or decay of diffuse dark matter particles in the Galactic halo can give excellent (for the  $W^+W^-$  channel) or at least good (for the double  $\tau^+\tau^-$  channel) fits to the broad excess. However, the annihilation cross-section is of the order of  $10^{-23} \text{ cm}^3 \text{ s}^{-1}$ , larger than required for obtaining the correct relic abundance when dark matter froze out. We then study whether the narrow peak at  $\sim 1.4$  TeV could be explained by a nearby subhalo, which thanks to the smaller distance, could supply  $e^+e^-$  within a narrow energy range. We find that in order to produce a peak width less than the DAMPE energy bin width (0.2 TeV), the source must be located within  $r \lesssim 0.53$  kpc. Our global fit models do not produce the peak-like feature, instead at  $\sim 1.4$  TeV the spectrum show either a slope or a cliff-like feature. However, if less than optimal fit to the data is allowed, the peak-like feature could be generated. Furthermore, an excellent fit with peak could be obtained with model B if the background is rescaled. If the dark matter decay and annihilation rates are determined using the broad excess, the required subhalo mass could be  $\sim 10^5 M_\odot$  for decay model with dark matter particle lifetime  $7.3 \times 10^{25} \text{ s}$ , or  $\sim 10^{4.5} M_\odot$  for annihilation model with cross-section  $10^{-23} \text{ cm}^3 \text{ s}^{-1}$  and a shallower density profile slope  $\alpha = 1.2$ , or  $\sim 10^{2.5} M_\odot$  if the density profile slope is as steep as  $\alpha = 1.7$ . However, considering the distribution profile of dark matter subhalos in our Milky Way's host halo, the probability for the existence of a such nearby subhalo as massive as given above is very low.

PACS numbers:

## I. INTRODUCTION

According to recent astronomical observations, about 26% of the total cosmic density is made up by non-baryonic dark matter, much more than the 4.7% baryonic matter we know of [1]. The dark matter plays a crucial role in large scale structure growth and galaxy formation, but its presence is only inferred from its gravitational effects, while its nature is still unknown. A simple and plausible conjecture is that the dark matter are made up of unknown particles, which are electromagnetically neutral but participate in weak interactions. Such dark matter particles may annihilate or decay into standard model particles. In the indirect search of weakly massive interacting particle (WIMP) dark matter, one looks for the signature of dark matter by observing  $\gamma$ -ray, energetic neutrino or charged cosmic ray (CR) particles as annihilation or decay products (for a review see e.g. [2]). As these are also produced by other astrophysical pro-

cesses, which are not always well understood, it is necessary to look for distinct signatures from the dark matter annihilation or decay processes. In the case of CR, most CR particles follow power-law distributions, which could be nicely explained as the result of diffusive shock acceleration by supernovae remnants (SNR), followed by a complicated transportation process in the Milky Way [3]. On the other hand, the dark matter particle has a specific mass, so the energy of particles produced in dark matter annihilation or decay would be distributed in a particular energy range, which may produce an excess or deviation from the simple power-law in the CR energy spectrum. In particular, if the dark matter particle could annihilate or decay directly to a pair of standard model particles, this may produce a narrow line feature, which would be a smoking gun signature of dark matter, as there is no other known mechanism to produce such narrow line feature in the multi-GeV energy range.

The CR electrons and positrons have been measured by a number of balloon or space-borne experiments. The HEAT [4], ATIC [5], PAMELA [6], Fermi [7, 8], and AMS-02 [9] have measured the electron and positron spectrum up to 2 TeV. An intriguing excess above a few tens GeV were found by these experiments, though

\*Co-first author

<sup>†</sup>Corresponding author

the uncertainty remains large at the high energy end where the CR flux drops. In addition, the ground based H.E.S.S. experiment observes the electron and positron spectrum indirectly at higher energies [10]. From joint analysis of these experiment, a possible break in the energy spectrum was found around TeV scale, though in such analysis the systematic uncertainty is sizable [11, 12]. Such an excess could be generated by dark matter annihilation or decay (e.g. [13–15]), but to obtain a large excess, the dark matter annihilation rate must be higher than usually assumed for achieving the correct abundance when it froze out in the early Universe, or are from a relatively nearby source such as a subhalo [10, 16–22]. Alternatively, the excess could be produced by some energetic astrophysical processes such as pulsars or SNRs which could inject energetic electrons or positrons in the CR energy spectrum [23–38].

The DAMPE satellite has made a new measurement of the electron and positron spectrum (electrons and positrons are not distinguishable in its observation). This satellite is designed to have low background contamination from the much greater proton component of the CR, and have high energy resolution so that sharp feature in the CR electron and positron spectrum would not be erased by energy resolution issue [39]. Recently, the DAMPE experiment has released their measurement from 25 GeV to 4.6 TeV [40]. Their energy spectrum is broadly consistent with the Fermi-LAT [41], however higher than those from the AMS-02 and CALET [42] at  $\gtrsim 70$  GeV. A break in the energy spectrum is indeed found at about 1 TeV, confirming the earlier result from H.E.S.S. experiment, and provides a very precise measurement of CR electron positron energy spectrum at the TeV energy range. These results raise new interests on the dark matter contribution to the CR electron and positron spectrum.

In addition to the break, there is also a single peak feature at  $\sim 1.4$  TeV, with a statistical significance of  $\sim 3\sigma$ . We should take a cautionary note here: the number of actual events detected in this energy bin is only 93, while for the two adjacent bins the numbers are 74 and 33 respectively, so it is possible that the large peak is due to a statistical fluctuation. This would become more clear in the future as more data is accumulated. Nevertheless, the peak is very intriguing, because in sources of astrophysical origin, such as SNRs or pulsars, it is not easy to generate particles with a single energy. So if the peak is real, it would be of great importance to the indirect dark matter search. Indeed, as we shall see below, even in the dark matter scenario it is not easy to produce a narrow peak in the charged particle spectrum, because the electrons and positrons produced in dark matter annihilation or decay will diffuse into broad energy distributions during their propagation. So to generate a narrow peak in the spectrum, the source must be located at a very small distance where the diffusion does not take long time. One such possibility is a dark matter subhalo which is accidentally located near the Solar system.

In this paper, we shall investigate the scenario that the dark matter annihilation or decay serve as possible source of the excess CR electrons and positrons in light of the new DAMPE data. The paper is organized as follows: In Sec. II we describe our method for computing the CR electron and positron spectrum. In Sec. III we present the results from fitting the broad spectral excess with the Galactic halo diffuse dark matter contribution. In Sec. IV, we study whether the peak feature at  $\sim 1.4$  TeV could be generated by a nearby subhalo. In Sec. V we investigate what is the required mass for such a subhalo, and the constraint on the model from inverse Compton scattered photons and CR anisotropy. We conclude in Sec. VI.

## II. METHODS

The propagation of charged CR particles in the Milky Way can be described as a diffusion process, with interaction with other particles, and energy loss by radiation and collision, as well as re-acceleration in the turbulent magnetic field [43]. To quantitatively model this process, the GALPROP<sup>1</sup> software package has been developed, which solves the propagation equation with a Crank-Nicholson implicit second-order scheme [44]. The primary electrons are mostly produced in SNRs. Their injection spectrum is modeled as a simple power-law form, as is expected from the diffuse shock acceleration mechanism [45]. In the propagation models, the source item of the primary electrons is also often described as a broken power-law spectrum multiplied by the assumed spatial distribution given in the cylindrical coordinate [44]. The density of CR electron source is modeled as an exponential disc. The secondary electrons and positrons are produced during collisions of CR nucleons (protons dominant) with the interstellar gas [46]. The distribution of the interstellar gas, which collide with CR particles and generate secondary particles, is derived from the observational data of H and CO, etc. [47, 48]. The CR propagation time can be constrained observationally by the ratio between primary particles and the secondary particles, such as the  $\text{Be}^{10}/\text{Be}^9$  and B/C ratios in the cosmic ray. Alternatively, with the advent of high quality data from the AMS-02 experiment, the CR model parameters may also be determined solely from the proton [49] and B/C [50] data of AMS-02, as is demonstrated first in Ref. [51], which yield tighter constraints. In this paper, we shall also follow this approach.

If some CR particles are produced by dark matter annihilation or decay, their propagation processes are the same, only the injection source distribution and energy spectrum differ. For dark matter annihilation, we model

---

<sup>1</sup> <https://galprop.stanford.edu/>

the source term as

$$q(\mathbf{r}, p) = \frac{\rho(\mathbf{r})^2}{2m_\chi^2} \langle \sigma v \rangle \sum_X \eta_X \frac{dN^{(X)}}{dp}, \quad (1)$$

where  $\langle \sigma v \rangle$  is the velocity-averaged dark matter annihilation cross-section multiplied by dark matter relative velocity (referred to as cross-section),  $\rho(\mathbf{r})$  is the dark matter density distribution function, and  $dN^{(X)}/dp$  is the injection energy spectrum of secondary particles from dark matter annihilating into standard model final states through all possible intermediate states  $X$  with  $\eta_X$  the corresponding branching fractions. Similarly, the source term for decay can be modeled as

$$q(\mathbf{r}, p) = \frac{\rho(\mathbf{r})}{m_\chi} \Gamma_\chi \sum_X \eta_X \frac{dN^{(X)}}{dp}, \quad (2)$$

where  $\Gamma_\chi$  is the decay rate. The density profile  $\rho(\mathbf{r})$  of the dark matter halos were derived in N-body simulation, such as NFW [52], isothermal [53], and Moore [54] models. In this paper we use the Einasto [55] profile to model the dark matter distribution. The energy spectrum of electrons and positrons of each channel is calculated by PYTHIA v8.175 [56]. The hadronic model interaction part of the code is also modified to improve the treatment of secondary particles [57].

In the dark matter particle annihilation or decay, the electrons and positrons can be produced directly, here we shall call this the direct  $e^+e^-$  channel. Note that the annihilation or decay may produce an  $e^+e^-$  pair, or either an  $e^+$  or an  $e^-$  plus other particles, but on the whole produce equal numbers of  $e^+$  and  $e^-$ . For our investigation these differences do not matter, though in the former case the energy of the electron or positron would be exactly  $m_\chi$  (annihilation) or  $m_\chi/2$  (decay), and the primary energy spectrum of electrons and positrons is a very narrow peak around  $E_0 = m_\chi$  (annihilation) or  $E_0 = m_\chi/2$  (decay) for the pair production. The electrons and positrons may also be produced by annihilation or decay into intermediate particles, such as the  $W^+W^-$  pairs or  $\tau^+\tau^-$  pairs, which further decay to produce electrons and positrons. In these cases the energies are generally more broadly distributed. In this paper we shall consider 1) model A: electrons and positrons are produced through the  $W^+W^-$  channel and the direct  $e^+e^-$  channel; and 2) model B: through the double  $\tau^+\tau^-$  channel and direct  $e^+e^-$  channel. In previous analysis, it has been found that in fitting the broad spectrum excess measured by the AMS-02 experiment, the other channels usually do not yield as good fit as the ones listed above [57]. The branching ratio of direct  $e^+e^-$  channel to  $W^+W^-$  channel (double  $\tau^+\tau^-$  channel),  $f$ , is treated as a free parameter to explore the favored final state.

According to their origins, we divide the CR electrons and positrons into three components : 1) an astrophysical background, this is the primary electrons from distant astrophysical sources and the secondary electrons

and positrons generated when these primary electrons propagate in the space between sources and observers; 2) a diffuse dark matter component, including the electrons and positrons produced by the annihilation or decay of the diffuse dark matter particles in the Galactic halo, and the secondary electrons and positrons generated during their propagation; 3) a component from a nearby subhalo, which may accidentally to be located at a very close distance so that it significantly alter the CR energy spectrum.

## A. The broad spectrum

Precise measurements of CR electrons and positrons were reported by the AMS-02 experiment [58]. They found that in the measured flux of electrons plus positrons, the positron fraction reaches the maximum of 15.9% at 305 GeV [59]. There is a positron excess against the astrophysical background, which is usually interpreted as produced by either pulsars or dark matter annihilation or decay [51, 60–63].

If equal amount of electrons and positrons at the same energy are produced by the additional sources such as pulsars, dark matter annihilation or decay, then by subtracting the same amount of electrons as positrons from the total spectrum, one can obtain the contribution of the astrophysical primary electrons. In Ref. [64], the primary electron background is extracted from the AMS-02 experiment, and it indeed follows a power law spectrum as expected for astrophysical origin. This knowledge of primary electrons in turn helps us to improve the understanding of the additional sources

In a recent work [57], it is found that the CR electrons and positrons background as measured by AMS-02 agrees well with the prediction by a convection and re-acceleration diffusion (DCR) model using the CR protons, positrons and B/C data of the same experiment. Based on the two-peaks feature of the CR electrons and positrons background spectrum, they further pointed out that the positron excess in AMS-02 experiment could be interpreted by diffuse dark matter annihilation in Galactic halo, and the most relevant channels are the  $W^+W^-$  (in the bosons and quarks) and double  $\tau^+\tau^-$  (in the leptons) annihilation channels.

The dark matter profile is chosen as Einasto [55], which is described approximately by a power-law density distribution:

$$\rho(r) = \rho_\odot \exp \left[ - \left( \frac{2}{\alpha_E} \right) \left( \frac{r^{\alpha_E} - r_\odot^{\alpha_E}}{r_s^{\alpha_E}} \right) \right], \quad (3)$$

with  $\alpha_E \approx 0.17$  and  $r_s \approx 20$  kpc. The local dark matter density is fixed at  $\rho_\odot = 0.43$  GeV cm<sup>-3</sup> [65]. In this model there is no nearby sources such as dark matter subhalos, and the CR electrons and positrons coming from the dark matter annihilation is a diffuse distribution in the Milky Way. The energy spectrum of electrons and positrons of each channel is calculated by PYTHIA

v8.175 [56]. Then based on the above density profile, the final energy spectrum after propagation is obtained via the GALPROP [66].

In this paper, we use the spectrum template generate as [57] for the  $W^+W^-$ , double  $\tau^+\tau^-$  and direct  $e^+e^-$  channels respectively, as the theoretical models for investigating the broad spectrum excess. We leave the normalizations and branching ratio as free parameters.

### B. Nearby source

Even for the dark matter origin scenario, typically the observed CR electron and positron spectrum would still be a broad bump rather than a narrow peak. Charged particles move in curved trajectories in the stochastic interstellar magnetic field, so their transportation in the Galactic-scale distance can be described as a diffusion process. The TeV electrons and positrons also lose their energy rapidly by synchrotron radiation and inverse Compton scattering, with a life time of  $10^5 \sim 10^6$  years. As a result, even if the electrons and positrons are produced at a single energy by dark matter annihilation or decay, the peak would still be broadened quickly as they propagate through the space. For the electron and positron spectrum to retain a narrow peak, the source must be fairly close by, so that the peak is not greatly damped by energy loss or momentum space diffusion during the propagation.

The N-body simulations show that in the Galactic dark matter halo there could be a large number of subhalos which were produced during the hierarchical structure formation process [67, 68]. Many of such halos did not form stars so they can not be observed directly (see Ref. [69] for a recent review). In what follows we compute the contribution to the electron and positron spectrum from a nearby subhalo, to see if the peak in the energy spectrum could be reproduced.

Although the CR spectrum from a nearby subhalo could also be simulated with the GALPROP code, in this paper we consider to use an analytical solution of the CR diffusion equation from a nearby source. While this is not as accurate and comprehensive as the GALPROP code, it allows more intuitive understanding of the physical picture.

We first assume the source produce electrons and positrons with a single energy  $E_0$ , from a point source. The propagation equation of primary CR electrons (ignoring secondary ones produced in particle collisions) can be written as

$$\begin{aligned} \frac{\partial \psi}{\partial t} = & \nabla \cdot (D_{xx} \nabla \psi - V_c \psi) + \frac{\partial}{\partial p} [p^2 D_{pp} \frac{\partial \psi}{\partial p}] \\ & - \frac{\partial}{\partial p} [\dot{p} \psi - \frac{p}{3} (\nabla \cdot V_c) \psi] + \mathbf{S} \end{aligned} \quad (4)$$

where  $\psi(\mathbf{r}, p, t)$  is the number density of electrons per unit energy,  $D_{xx}$  and  $D_{pp}$  are the spatial and momentum diffusion coefficients respectively,  $V_c$  the bulk velocity,

and  $\mathbf{S}$  the source distribution. For the present problem,  $p \approx E$ . This is a linear equation, so we may solve the subhalo contribution separately, and just adding it to the solution for the whole galaxy.

The diffusion coefficient and other parameters in the cosmic ray propagation model were fitted from other observations [70],  $D_{xx} = D_0 (\rho/\rho_0)^\delta$ , where  $D_0 = 6.59 \times 10^{28} \text{ cm}^2 \text{ s}^{-1}$ ,  $\rho = pc/Ze$  and  $\rho_0 = 4 \times 10^3 \text{ MV}$ , here we take  $\delta = 1/3$  which is for Kolmogorov spectrum of interstellar turbulence. In the TeV energy range, the electrons and positrons lose their energy primarily by synchrotron radiation and inverse Compton scattering (ICS). The energy loss rate for relativistic electrons via synchrotron radiation is

$$-\left(\frac{dE}{dt}\right)_{\text{syn}} = 6.9 \times 10^{-25} \gamma^2 \left(\frac{B}{\mu\text{G}}\right)^2 [\text{GeV s}^{-1}], \quad (5)$$

where  $\gamma = E/m_e c^2$ , and  $B$  is the magnetic field in units  $\mu\text{G}$  and we adopt the typical magnetic field  $\sim 6 \mu\text{G}$  in the Solar neighborhood [71].

Regarding the ICS, the Klein-Nishina cross-section for the electron-photon scattering is [72]

$$\sigma_{\text{KN}}(\mathcal{E}, \mathcal{E}_0, \gamma) = \frac{3\sigma_T}{4\gamma^2 \mathcal{E}_0} G(q, \Gamma_e), \quad (6)$$

where  $\mathcal{E}_0$  and  $\mathcal{E}$  are the energy of photons before and after scattering.  $\sigma_T = 6.65 \times 10^{-25} \text{ cm}^2$  is the Thompson scattering cross-section. The function

$$G(q, \Gamma_e) = 2q \ln q + (1 + 2q)(1 - q) + \frac{(\Gamma_e q)^2 (1 - q)}{2(1 + \Gamma_e q)}, \quad (7)$$

where

$$\Gamma_e = \frac{4\mathcal{E}_0 \gamma}{m_e c^2}, \quad q = \frac{\mathcal{E}}{(\gamma m_e c^2 - \mathcal{E}) \Gamma_e}. \quad (8)$$

The spectrum of the up scattered photons is

$$\frac{dN}{dt d\mathcal{E}} = \int \sigma_{\text{KN}} \frac{dU_{\text{rad}}}{\mathcal{E}_0 d\mathcal{E}_0} d\mathcal{E}_0, \quad (9)$$

and the energy loss rate via ICS

$$-\left(\frac{dE}{dt}\right)_{\text{ICS}} \approx \int_{\mathcal{E}_0}^{\mathcal{E}_{\text{max}}} \mathcal{E} \frac{dN}{dt d\mathcal{E}} d\mathcal{E}, \quad (10)$$

the integration is performed to the maximum energy of the up scattered photons,

$$\mathcal{E}_{\text{max}} = \frac{4\mathcal{E}_0 \gamma^2}{1 + 4\mathcal{E}_0 \gamma / (m_e c^2)}. \quad (11)$$

From [73, 74], near our Solar system, the interstellar radiation field has three peaks at the NIR ( $\sim 1 \mu\text{m}$ ), FIR ( $\sim 100 \mu\text{m}$ ) and CMB ( $\sim 1000 \mu\text{m}$ ), with energy density  $\sim 0.4 \text{ eV cm}^{-3}$ ,  $\sim 0.3 \text{ eV cm}^{-3}$  and  $\sim 0.2 \text{ eV cm}^{-3}$  respectively. Adopting these values we have

$$-\left(\frac{dE}{dt}\right)_{\text{ICS}} \approx \sum_i \int_{\mathcal{E}_{0,i}}^{\mathcal{E}_{\text{max},i}} d\mathcal{E} \frac{3\sigma_T c U_{\text{rad},i}}{4\gamma^2 \mathcal{E}_{0,i}^2} G(q_i, \Gamma_{e,i}) \quad (12)$$

where  $i$  is one of NIR, FIR or CMB respectively.

The final energy loss rate is

$$b = -\frac{dE}{dt} = -\left(\frac{dE}{dt}\right)_{\text{syn}} - \left(\frac{dE}{dt}\right)_{\text{ICS}}. \quad (13)$$

For example, at 1.5 TeV,  $b \approx 3.1 \times 10^{-10} \text{ GeV s}^{-1}$ . Also, if the source is nearby, the diffusion in momentum space which is due re-acceleration can be neglected, as  $\frac{D_{pp}}{E} \sim 6.2 \times 10^{-15} \text{ GeV s}^{-1} \ll b$ .

The dynamical time scale of the Milky Way is of order of  $10^8$  year, so the time scale for the subhalo to pass by is much longer than the life time of the electrons and positrons. We may then assume a steady state for the CR spectrum is reached,  $\partial\psi/\partial t = 0$ . We ignore the bulk velocity  $V_c$ . For a point source of monochromatic electron or positron injection,  $\mathbf{S} = Q\delta(\mathbf{r})\delta(E - E_0)$ , then the propagation equation could be simplified as

$$D_{xx}\nabla^2\psi + b\frac{\partial}{\partial E}\psi + Q\delta(r)\delta(E - E_0) = 0. \quad (14)$$

This equation can be solved by making a 3D Fourier transform over the spatial dimensions and a 1D Laplace transform over time. If the source is very nearby, we do not need to consider the global confinement to the Galactic disk by the magnetic field. The solution in the spherically symmetric case is given by

$$\psi(E_0, E, r) = \frac{Q}{b} \frac{\exp[-\frac{(4\pi D_{xx}/b)(E_0 - E)}{r^2}]}{[(4\pi D_{xx}/b)(E_0 - E)]^{3/2}}. \quad (15)$$

Then the observed specific intensity of particles number flux is  $J \approx \psi c/(4\pi)$ .

If the injected electrons and positrons are not of a single energy but has an energy distribution of  $dN/dE$  (e.g. for  $W^+W^-$  channel or double  $\tau^+\tau^-$  channel), the corresponding spectrum could be obtained by

$$J = \frac{cf}{4\pi(1+f)} \int dE' \frac{dN}{dE'} G(E', E, r) \quad (16)$$

where the Green function  $G(E', E, r)$  is given by Eq. (15). If the annihilation or decay has both direct  $e^+e^-$  channel and other channels, the result is given by the sum of all the channels.

We show the electron and positron spectrum produced via the different channels in Fig. 1, for model A (top panel) and model B (bottom panel). Here we fix  $E_0 = 1.5$  TeV and  $f = 0.01$ . In each case we show the results for  $r = 0.1$  and 1 kpc. The total injection rate  $Q$  are adjusted ( $Q = 10^{33}$  and  $10^{36} \text{ s}^{-1}$  for  $r = 0.1$  and 1 kpc respectively) so that the curves can be show on the same plot. As we expect, the closer the source, the narrower the peak. For  $r = 0.1$  kpc (blue) the peak is very sharp, while for  $r = 1$  kpc (red) the peak is a much broader one. Compared with the direct production case, the electrons and positrons produced via the  $W^+W^-$  or double  $\tau^+\tau^-$  channel have broader distributions, as the electrons and

positrons produced in this channel are not monochromatic. Moreover, the peak is located at higher energy for the  $r = 0.1$  kpc (blue) case than the  $r = 1$  kpc (red) case. If we want to generate a peak in the spectrum, the direct  $e^+e^-$  channel must be used.

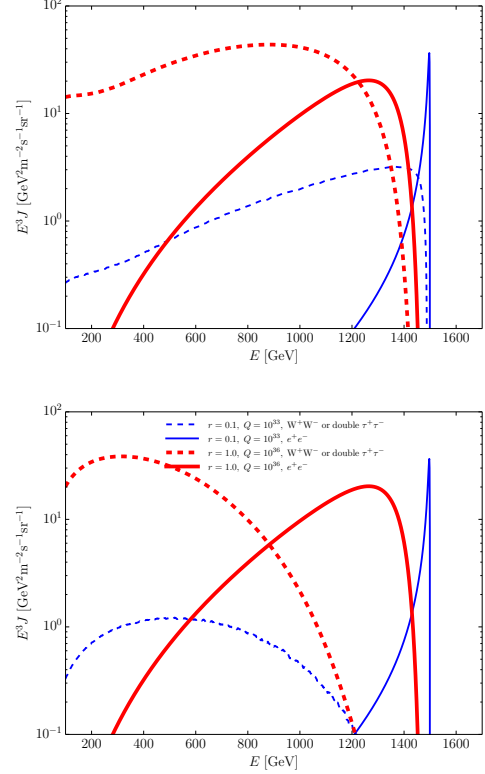


FIG. 1: The specific intensity of the electrons and positrons number flux from a nearby subhalo with different distances. Top panel is for model A while bottom panel is for model B.

We fit the normalization  $A$  of the broad spectrum of electrons and positrons due to  $W^+W^-$  or double  $\tau^+\tau^-$  channel and the branching ratio  $f$  of the direct  $e^+e^-$  channel to the  $W^+W^-$  or double  $\tau^+\tau^-$  channel, the distance  $r$ , and the amount of injection  $Q$  from the statistics:

$$\chi^2(A, f, r, Q) = \sum \frac{[\langle J_i^{\text{nr}}(f, r, Q) \rangle + \langle J_i^c(A, f) \rangle - J_{\text{obs}}^i]^2}{\sigma_{\text{stat},i}^2 + \sigma_{\text{sys},i}^2}, \quad (17)$$

where  $\langle J_i^{\text{nr}}(f, r, Q) \rangle$  is the average (i.e. integrating the intensity in the energy bin then divided by the bin width) mean intensity from the nearby source in the  $i$ -th energy bin; while

$$J_i^c(A, f) = A J_{W/\tau}^{\text{br}} + f A J_e^{\text{br}} + J_{\text{bg}}. \quad (18)$$

The astrophysical background  $J_{\text{bg}}$ , the broad spectrum template from the annihilation or decay of Galactic diffuse dark matter through the  $W^+W^-$  or double  $\tau^+\tau^-$  channel,  $J_{W/\tau}^{\text{br}}$ , and through the direct  $e^+e^-$  channel,  $J_e^{\text{br}}$ , are all generated using the algorithm presented in [57].

For simplicity we fix  $E_0 = 1.5$  TeV. Adopting a different value within  $\sim 0.1$  TeV does not change our result.

### III. FITTING WITH THE BROAD SPECTRUM

The CR electron and positron spectrum has been measured by a number of experiments, such as the VERITAS [75], H.E.S.S. [76, 77] and Fermi-LAT [41] before the DAMPE data release. These observations indicate a remarkable break in the spectrum at TeV scale. However, the electron and positron data from the ground based atmospheric Cherenkov telescopes such as H.E.S.S. have large uncertainties from the subtraction of hadronic background and discrimination against gamma rays events [76]. In detail, the very-high-energy flux of H.E.S.S. electrons is described by an exponentially cutoff power law with an index of  $3.05 \pm 0.02$  and a cutoff at  $2.1 \pm 0.3$  TeV in the range of 700 GeV to 5 TeV [76]. The low-energy extension of the H.E.S.S. electron measurement are from 340 GeV to 1.7 TeV with a break energy at about 1 TeV [77].

The TeV break of CR electrons and positrons are now confirmed by the highly precise DAMPE observation. If we assume the primary electron is described by a power-law, while the excess electrons and positrons have the same spectral distribution, the degeneracy between the background and excess can be broken, and the origin of the TeV break is connected to the positron excess [78]. This is confirmed in [64] where the features of the primary electron spectrum is carefully studied, which showed a power-law primary electron spectrum without TeV break.

Here, we derive the excess of electrons under the assumption that the number of excess electrons and positrons are the same. We use the AMS-02 experiment  $e^- - e^+$  data [58] to derive the primary electrons and the astrophysical background, and then subtract this background from the DAMPE data to obtain the excess<sup>2</sup>. The primary electrons and the background are shown as green dotted and black solid lines in each panel of Fig. 2. At  $\gtrsim 100$  GeV they are of similar power-law forms, implying that the amount of secondary electrons and positrons generated during the CR propagation is small. Our model background is consistent with Fermi-LAT, CALET and DAMPE observational constraints at

least at  $\lesssim 5$  TeV. At higher energies, the power-law background may break and decrease faster due to more efficiency energy loss in both injecting sources and during propagation process in Milky Way. At present the higher energy observations still have very large uncertainties, so we only use the background value at  $\lesssim 5$  TeV to interpret the DAMPE data.

We then compute the excess produced by diffuse dark matter particle annihilations in the Galactic halo. We consider the annihilation to electrons and positrons via the  $W^+W^-$  channel and direct  $e^+e^-$  channel (model A) or via the double  $\tau^+\tau^-$  channel and direct  $e^+e^-$  channel (model B).

In Fig. 2, we show dark matter annihilation model fit to the DAMPE measured spectrum data. We plot the primary electrons derived from the AMS-02  $e^- - e^+$  data, the derived background, the dark matter contribution, and the dark matter plus background total. The top two panels show the model A results, while the bottom two show the model B results. In the left panels of Fig.2, we try to fit all data points including the peak point in the DAMPE data, while in the right panels we exclude the peak point. For model A, by excluding the peak point, the fit to the other points is improved. For model B there is steep drop of the spectrum at  $E_0 = m_\chi$ , where  $m_\chi$  is the dark matter particle mass. This cliff-like edge fits the peak point better, however the fitting is worse for the energy just below  $E_0$ .

We see all these models provide good fit to the data, at least at  $\gtrsim 100$  GeV. For model A the  $\chi^2_{\min}/\text{d.o.f} = 1.24$  and  $1.48$  when we include or exclude the 1.4 TeV peak data respectively. For model B, the corresponding  $\chi^2_{\min}/\text{d.o.f} = 2.33$  and  $2.10$ . The model A fit is better than model B, particularly because at the lower energy part, its spectral shape agrees with the data very well.

The best-fit dark matter particle mass are 1.7 TeV and 1.3 TeV respectively for the left and right panel, for model A, and 1.4 TeV and 1.2 TeV respectively for model B. The required annihilation cross-sections are typically  $\langle\sigma v\rangle \sim 10^{-23} \text{ cm}^3 \text{ s}^{-1}$ , within the constraints derived from the AMS-02 electron data [60]. The cross-section values are however larger than the one required to get correct abundance of WIMPs during the thermal decoupling. To obtain large abundance, the dark matter must be produced non-thermally in the early Universe, or the cross-section of its annihilation in the current time must be somehow enhanced [16, 17]. Moreover, while the cross-section is derived for electrons and positrons production, we note that these are larger than the observational limits on cross-section of annihilation into photons derived from observations of the dwarf spheroidal galaxies [79, 80]. The required cross-sections here are one order of magnitude greater than those of VERITAS [79], and three order larger than the one from Fermi-LAT [80]. Although the cross-sections of  $\gamma$ -ray and electrons and positrons could be different in principle, we expect them to be of the same order, and special mechanism may be needed to achieve the large cross-section to electrons and positrons while

<sup>2</sup> A caveat: there are discrepancies between the CR electrons measured in the various experiments, including AMS-02, Fermi-LAT, DAMPE and CALET, and the origin of such discrepancies is not clear, so there is no fully self-consistent way to use these measurements jointly. In our treatment below, counting on the fact that the AMS-02 has the capability of distinguishing electrons and positrons, and the best precision in the CR electron flux measurement, we use its data to derive the astrophysical background, but still there is the risk that the excess may be overestimated. An alternative treatment is discussed in Sec. IV C.

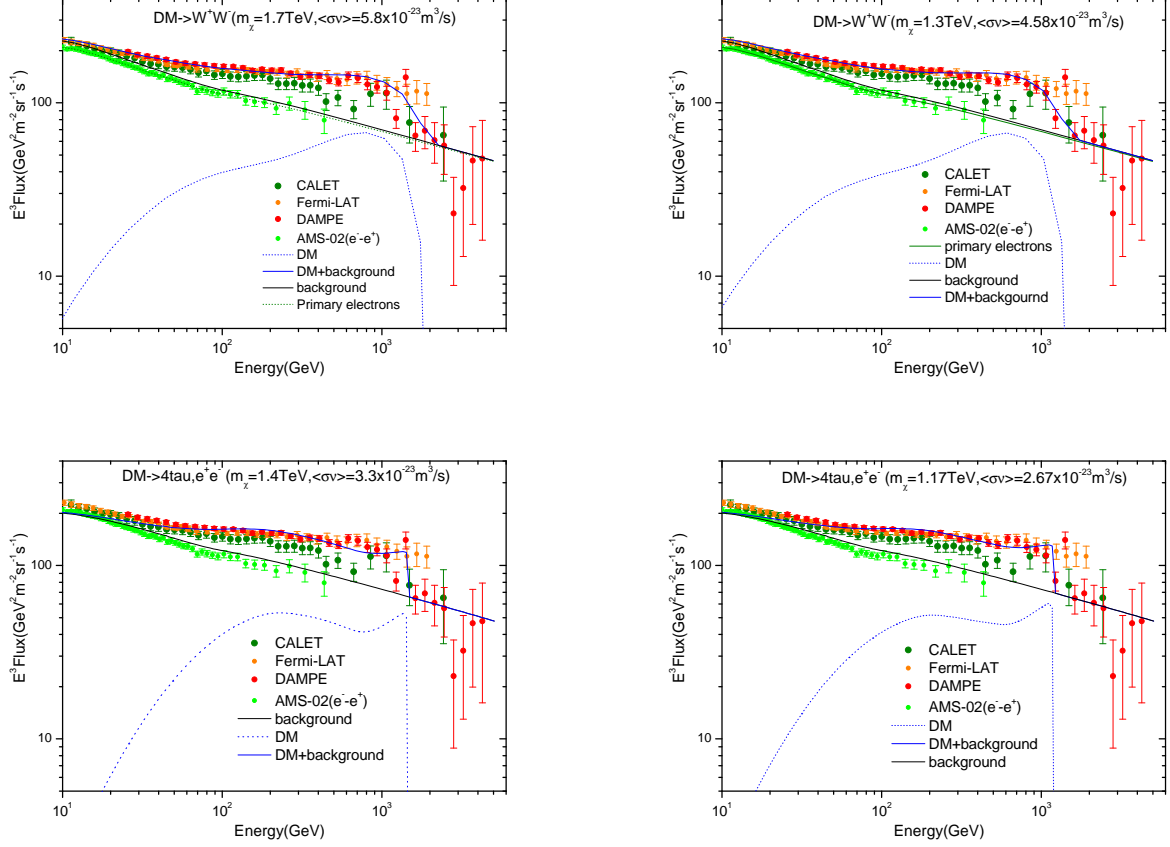


FIG. 2: The primary electrons background derived from  $(e^- - e^+)$  of the AMS-02 data [59] and the total flux of CR electrons and positrons background measured by DAMPE. The curves that fit the data including and excluding the peak point near 1.4 TeV are shown in the left and right panel respectively. We write the best-fit dark matter particle mass  $m_\chi$  and the velocity weighted cross-section  $\langle\sigma v\rangle$  in each panel. For top panels, the  $\chi^2/\text{d.o.f} = 1.24$  (left) and 1.48 (right) respectively, while for the bottom panels  $\chi^2/\text{d.o.f} = 2.33$  and 2.10 respectively.

not violating the  $\gamma$ -ray bound.

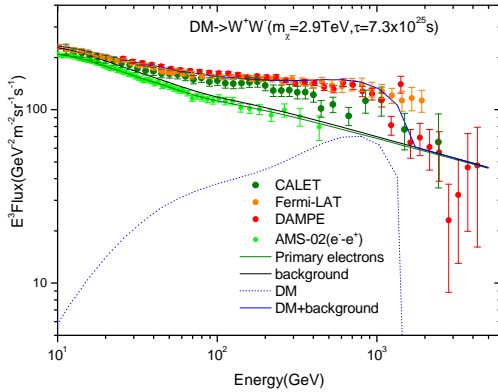


FIG. 3: Spectrum for dark matter decay via the  $W^+ W^-$  case.

In the above we have discussed the case of annihilations. In the case of decay, except for the mass which is doubled and the rate is determined from decay life time instead of the annihilation cross-section, others are similar. In Fig. 3 we show the spectrum of the decay in model A. The spectrum is very close to that of the annihilations, though dark matter particle mass is doubled with  $m_\chi = 2.9$  TeV. The life time of the decaying particle is  $\tau = 7.3 \times 10^{25}$  s.

In principle, the dark matter annihilation and decay results may differ, because the annihilation rate  $\propto n^2$ , while the decay rate  $\propto n$ , where  $n$  is the number density of dark matter particles, so the source distribution is in principle different. Nevertheless, in the end we find that the results are not much different in this case. As the spectrum for the two cases are quite similar, we shall mainly discuss the annihilation, though most of the results are also applicable to decays.

#### IV. THE PEAK AND NEARBY SOURCE

In the last section we see that the Galactic halo diffuse dark matter annihilation could provide a reasonably good fit to the DAMPE  $e^+e^-$  spectrum, though it does require a very large annihilation cross-section. However, there is no peak produced in the spectrum. Here, we tentatively treat the peak as real, and consider whether such a peak could be produced in dark matter annihilation or decay from a nearby subhalo. To do this, we use the GALPROP code to compute the primary background and diffuse dark matter contribution from the Galactic halo, then adding the contribution from the nearby subhalo. The dark matter parameters and subhalo parameters are varied to fit the DAMPE spectrum.

##### A. Global Fit Models

First we consider the two models introduced in Sec. II: model A, in which the  $e^+e^-$  are produced by the direct channel and the  $W^+W^-$  channel; and model B, in which the  $e^+e^-$  production are from the direct channel and the double  $\tau^+\tau^-$  channels. The branching ratio of the direct channel to other channels are taken as free parameters.

**Model A.** In Fig.4, we plot the best fit to the DAMPE spectrum. The CR background, the various contributions from dark matter annihilations, and the total of these are all plotted in the figure. As we can see from the figure, there is no peak in the total spectrum curve, which behaves as a gentle break, despite the fact that a subhalo is introduced. Looking into the details, we see the  $W^+W^-$  channel broad spectrum (i.e. the one from Galactic halo diffuse dark matter annihilations) gives an excellent fit to the broad excess, which are the majority of the data and also have much smaller measurement error bars than the few data points near the 1.4 TeV peak. As a result, the  $W^+W^-$  channel is the dominant contribution to the DAMPE spectrum. The broad  $e^+e^-$  spectrum (i.e. the direct channel contribution from the Galactic halo diffuse dark matter), on the other hand, does not have the correct shape to fit the broad excess, so its contribution must be suppressed. We plot the  $\log f - \log A$  distribution in Fig. 5, with other parameters marginalized. We find that the branching ratio is limit to be  $f \lesssim 1.1 \times 10^{-4}$  at  $3\sigma$ , meaning that the contribution from direct  $e^+e^-$  channel is quite limited compared with the  $W^+W^-$  channel. Thus, the whole spectrum shape is determined by the  $W^+W^-$  channel. The branching ratio of the direct channel to the  $W^+W^-$  channel  $f$  is however a single parameter, so the direct  $e^+e^-$  channel from the subhalo which has the desirable spectral shape of a peak is also suppressed. The final spectrum fits most of the data, but does not have a peak, and is not significantly better than the broad spectrum fit given in Sec. II.

Is it possible for the direct  $e^+e^-$  channel to dominate over the  $W^+W^-$  channel? Unfortunately, for realistic parameters for CR propagation and dark matter halo, the

Galactic halo diffuse dark matter annihilation via direct  $e^+e^-$  channel produce fairly hard spectrum, even after the diffusion process, as shown by the cyan colored curve in Fig. 4. The curve is broader than that of the nearby subhalo contribution, but still too narrow to produce the broad excess.

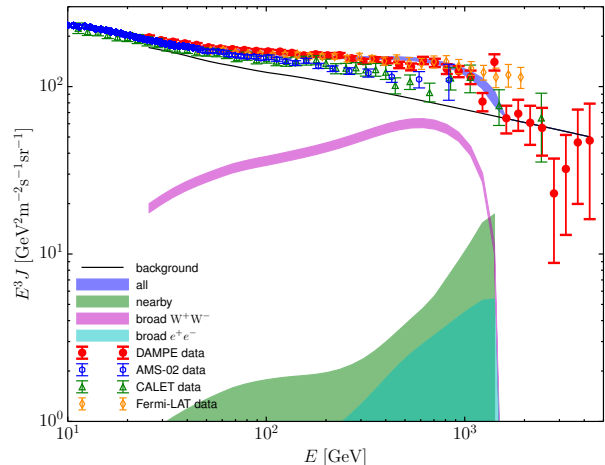


FIG. 4: The fit to DAMPE spectrum with model A, with various contributions shown and marked. The envelope corresponds to  $1\sigma$  in parameter space. As comparisons we also plot the Fermi-LAT, CALET and AMS-02 data.

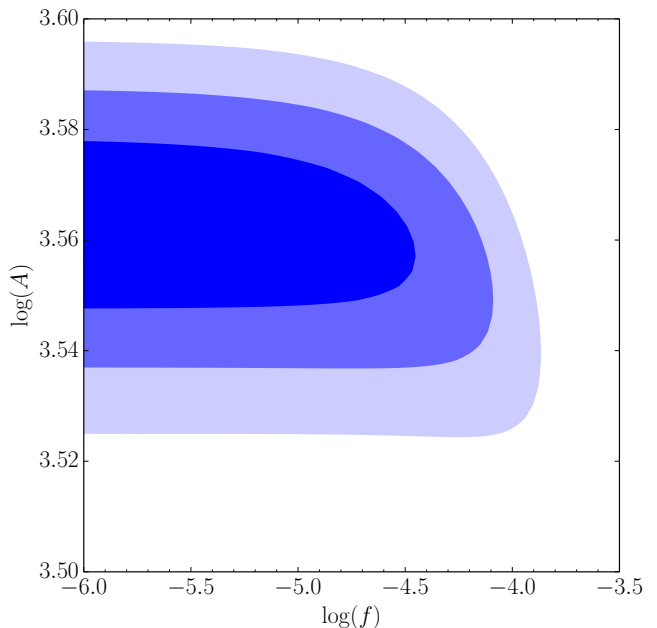


FIG. 5: The constraints on  $f$  and  $A$  for model A.

**Model B.** In Figs. 6 and 7 we show the corresponding results for model B. In this case, the fitting curve passes



closer to the peak point, but the spectral shape is more like a cliff than a peak, the flux on the left side of the peak is over-predicted. In fact, in this model the main contribution to the 1.4 TeV spectrum is not from the nearby subhalo, but instead from the direct  $e^+e^-$  channel component in the broad spectrum, i.e. from the Galactic halo diffuse dark matter annihilation or decay. Another problem is that the flux at energy around several tens GeVs are under predicted. Though the deviation is not very obvious on this plot, the measurement error in that energy range is much smaller. In this model, we obtain  $5.6 \times 10^{-4} \lesssim f \lesssim 1.2 \times 10^{-3}$  at  $3\sigma$ .

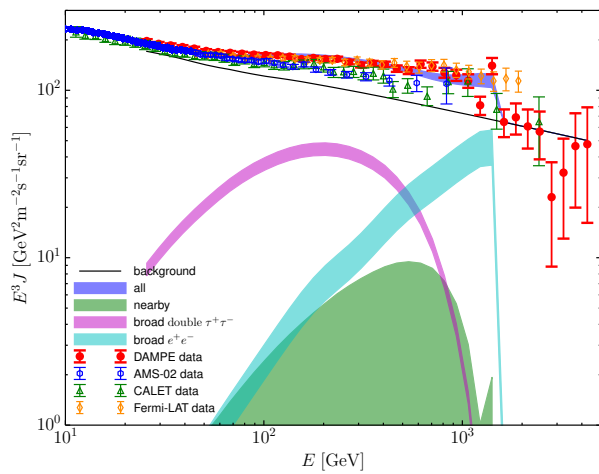


FIG. 6: Same as Fig. 4, but for model B.

In all these global fit models, the contribution from a possible nearby subhalo is limited to  $\lesssim 10 - 20\%$ . This small contribution is not or just barely apparent in the total flux, and fails to produce the peak-like feature.

### B. Eye Ball Fit Models

In the above we have seen that even with nearby subhalo, the global fit models do not produce a sharp peak in the spectrum. Here we consider how such a peak might be generated if we relax the requirement on the fit.

The different components have different spectral shapes. The background electrons have a simple power law shape and its normalization is determined by using the positron spectrum measured in the AMS-02 experiment. The direct  $e^+e^-$ ,  $W^+W^-$  and double  $\tau^+\tau^-$  channels from the Galactic halo diffuse dark matter annihilation also have essentially fixed spectral shape, though it depends on the Galactic halo model and the CR propagation parameters. The normalization of these depends on the dark matter annihilation cross-section or decay rate. In fact, the shapes are slightly different for the case of annihilation and the case of decay, as the radial profile of production in the Galactic halo are different, though

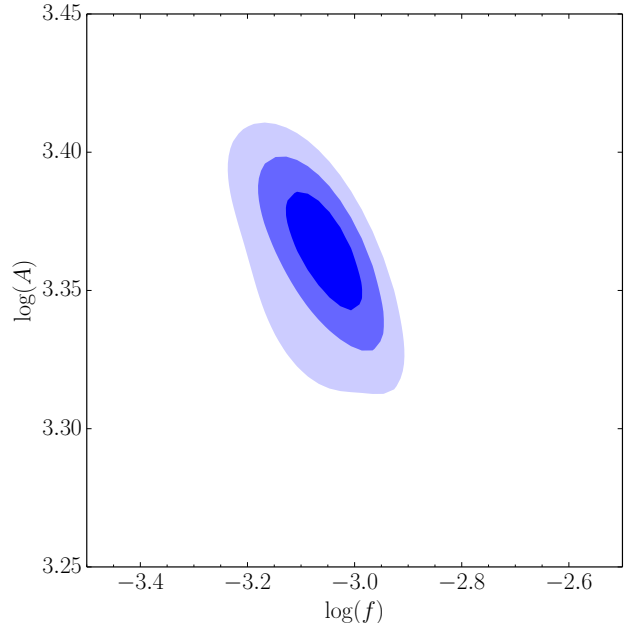


FIG. 7: Same as Fig. 5, but for model B.

we find that the difference is not large. On the other hand, for the nearby components the shape depend on the distance of the subhalo. This change is most obvious for the direct  $e^+e^-$  channel. By adjusting the branching ratio, one could change the relative contributions of the direct,  $W^+W^-$  and double  $\tau^+\tau^-$  channels, and by adjusting the subhalo distance and mass, one could change the relative contribution from the subhalo and the Galactic halo. The various different components are summed up to produce the total spectrum.

We note that the measurement error on the spectrum is smaller at lower energy scales. When performing a global fit with natural weight according to Eq. (17), the low energy part of the spectrum would largely determine the fit, that is the reason why the contribution of the direct  $e^+e^-$  component is strongly suppressed in the above, because the shape of broad (i.e. Galactic diffuse dark matter) direct  $e^+e^-$  component does not fit the lower energy part of the spectrum. This is also why the  $W^+W^-$  component is strongly favored, because its shape agrees extremely well with the observed excess. Here, to study whether a peak feature can be generated, we will give up the minimal variance fit based on the  $\chi^2$ , but use an “eye ball fit” to produce the spectrum. Note that even though the spectrum may appear to the eye to fit the data well, the actual  $\chi^2$  value would be much larger than the global fits we obtained above.

In performing the “eye ball fit”, we shall ignore the data above 2 TeV, where a dip appeared in the  $E^3 \times \text{Flux}$  plot. In this part the error is too large to draw definite conclusions.

**Model A.** Since the broad (diffuse dark matter in

Galactic halo)  $W^+W^-$  component has a shape very well suited for fitting the broad spectrum excess, we try to produce a spectrum with the broad and nearby (sub-halo)  $W^+W^-$  components as principal contributions in addition to the background. We have tried various combination of the two, and show one example of such “eye ball fit” in Fig. 8. We see the broad  $W^+W^-$  has a relatively flat shape up to 0.7 TeV, above which it drops rapidly. By contrast, the nearby  $W^+W^-$  source produce a one sided peak at  $\sim 1.4$  TeV, it drops to zero above 1.4 TeV, while declines rapidly at smaller 1.4 TeV. If we adjust the relative contribution of the two, we could create a slight hill in the spectrum at the desired position. However, we see that the hill has a gentle slope on the left side, though on the right side it could be very steep. Also, on the low energy part the fit is not good: it is obviously below the data point. To get a better fit on the low energy part, one has to increase the amplitude of the broad  $W^+W^-$  component. This can be achieved by increasing the annihilate cross-section or decay rate, but then the nearby source component would also increase, increasing the peak height while keep the same shape. If one wants to maintain the height by reducing the nearby source component (this can be done by adjusting the sub-halo mass), the relative amplitude of the two components will be changed, and the slope below 1.4 TeV would be even more gentle, making the peak disappear into a one sided slope, which is essentially the result of global best fit of model A above.

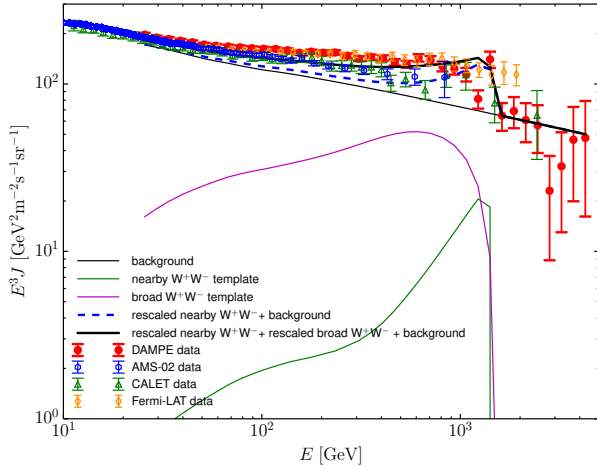


FIG. 8: An eye ball fit to the DAMPE spectrum with principal contribution from the broad and nearby  $W^+W^-$  components.

**Model B.** Next we consider the fit with the direct  $e^+e^-$  channels. The advantage of this channel is that the nearby source of this channel may generate very sharp peak, though its broad component has the wrong shape to fit the broad excess. If we relax the fit to the broad excess though, we could produce a peaked spectrum in this case. The double  $\tau^+\tau^-$  components which have flat-

ter shapes may also be employed to help improve the fit to the low energy broad excess part. An “eye ball fit” is shown in Fig. 9. Here we see the total spectrum (marked as “adjusted spectrum”) can well reproduce the peak feature at 1.4 TeV. This peak feature is dominated by contribution from the direct  $e^+e^-$  channel of nearby source. Interestingly, the direct  $e^+e^-$  from the diffuse dark matter in Galactic halo, the double  $\tau^+\tau^-$  from the diffuse dark matter together make up the contribution to the broad excess at a few hundred GeVs. Nevertheless, the total spectrum at below the few hundred GeVs are still significantly below that of observations. If one wants to improve the fit to that part from these components, however, one would have to increase the double  $\tau^+\tau^-$  contribution, which would again make the peak change into a slope or cliff, as the case of global fit model B.

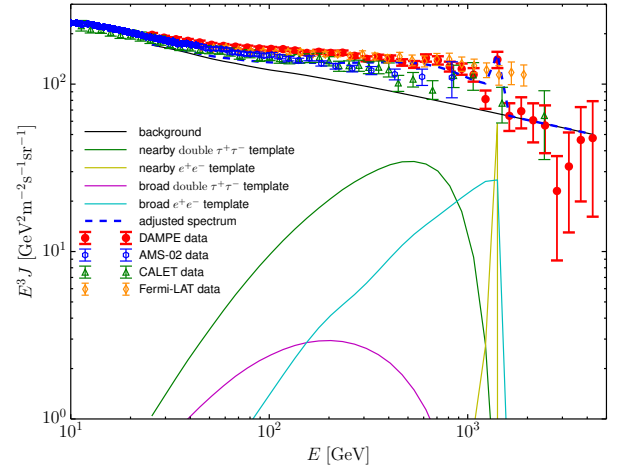


FIG. 9: An eye ball fit to the DAMPE spectrum with principal contribution from the broad and nearby double  $\tau^+\tau^-$  and direct  $e^+e^-$  components.

### C. Rescaled Background Model

In our analysis of the DAMPE data, we distinguish the “background”, which is the part of the spectrum contributed by normal astrophysical sources, and the excess, which we attribute to the contribution of dark matter. In the above we have used the experimentally derived background from the AMS-02 experiment. Here we rescale the experimentally derived background by a factor  $1.13 \times \exp(-E/5\text{TeV})$ , to explore the possibility that whether required dark matter contribution could be reduced and whether the  $4\tau$  channel could still fit the DAMPE data.

With this change, the fit to the broad excess can be significantly improved for the model B. We show the fit to the model with the rescaled background in Fig. 10. Here, compared with the global best fit model of

the original background, the reduced  $\chi^2$  of the best fit model decreased from 2.2 to 0.7. This is because with the rescaled background, the shape of the double  $\tau^+\tau^-$  components have much better match with the broad excess. The best fit model still does not show the narrow peak, but a model with the narrow peak is only slightly worse fit to the model than the best fit one. See the green dashed line in Fig. 10.

This example shows that we have to view the various fits with some caution. Systematic uncertainty such as the definition of the background could be very important in our interpretation of the data.

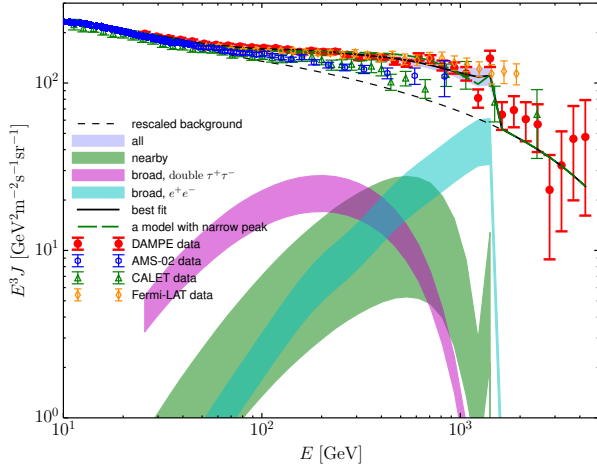


FIG. 10: A fit to the DAMPE spectrum with adjusted background, for the direct  $e^+e^-$  and double  $\tau^+\tau^-$  channels.

#### D. A background consistent with the H.E.S.S. 2017 data at $\gtrsim 5$ TeV

In the models described so far, we have not considered the constraints from the cosmic ray observations at energies above 5 TeV, because these data still have quite large uncertainties. Here we consider an astrophysical background with the inclusion of the H.E.S.S. 2017 data<sup>3</sup>, which results in softer spectrum than those used above. It drops dramatically at  $\gtrsim 40$  TeV due to the energy loss in propagation through the Milky Way. Similar to Sec. III, we first investigate a model that only includes the diffuse dark matter annihilation from the Galactic halo, to fit the DAMPE broad spectrum excess. We investigate many channels and find model A channels are still the best. The results for model A channels are shown in Fig. 11. The best-fit dark matter particle mass  $m_\chi = 1.9$

TeV and best-fit cross-section  $\langle\sigma v\rangle = 8.7 \times 10^{-23} \text{ cm}^3 \text{ s}^{-1}$ , close to the model A in Sec. III, which is 1.7 TeV and  $5.8 \times 10^{-23} \text{ cm}^3 \text{ s}^{-1}$ , see the top left panel of Fig. 2. Here we get  $\chi^2_{\min}/\text{d.o.f} = 1.1$ .

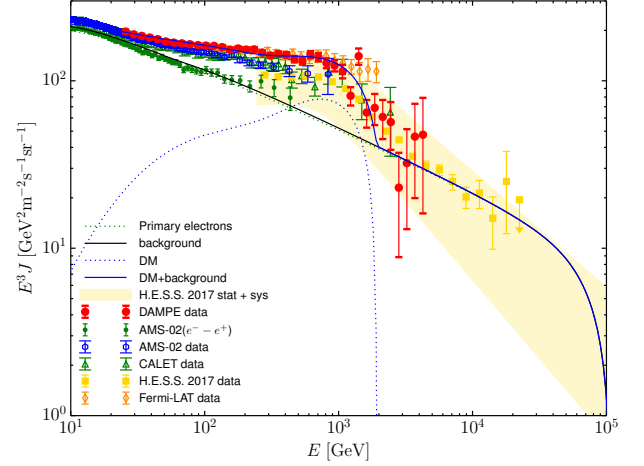


FIG. 11: A fit to the DAMPE spectrum with H.E.S.S. 2017 data consistent background, for the  $W^+W^-$  and direct  $e^+e^-$  channels.

We then include the nearby source and perform the fitting again as model A in Sec. IV. We fix dark matter particle mass to be 1.5 TeV. The results are shown in Fig. 12. Although adopting a different astrophysical background, we get similar conclusions: the annihilation of the diffuse dark matter in Galactic halo via  $W^+W^-$  channel could explain the broad spectrum excess very well, however the direct  $e^+e^-$  channel contributes negligibly; even introducing a nearby source, it is still not easy to generate a sharp peak near the 1.4 TeV.

## V. THE SUBHALO

We now consider the subhalo which can produce the peak shown above. We let the electrons and positrons of a subhalo plus the background fit the points near the peak.

### A. Decaying dark matter subhalo

For decaying dark matter with mass  $m_\chi = 2E_0$ , and the lifetime  $t_\chi$ , the injection rate is

$$Q_{\text{decay}} = \frac{2M_{\text{sub}}}{m_\chi t_\chi} = \frac{M_{\text{sub}}}{E_0 t_\chi} = 2.6 \times 10^{39} \frac{M_{\text{sub}}}{E_0 t_\chi} \text{ s}^{-1}, \quad (19)$$

where  $M_{\text{sub}}$  is subhalo mass in units of solar mass,  $E_0$  in units GeV and  $t_\chi$  in units Universe age ( $4.4 \times 10^{17} \text{ s}$ ). If we adopt the life time value  $7.3 \times 10^{25} \text{ s}^{-1}$ , in which

<sup>3</sup> <https://indico.snu.ac.kr/indico/event/15/session/5/contribution/694/material/slides/0.pdf>

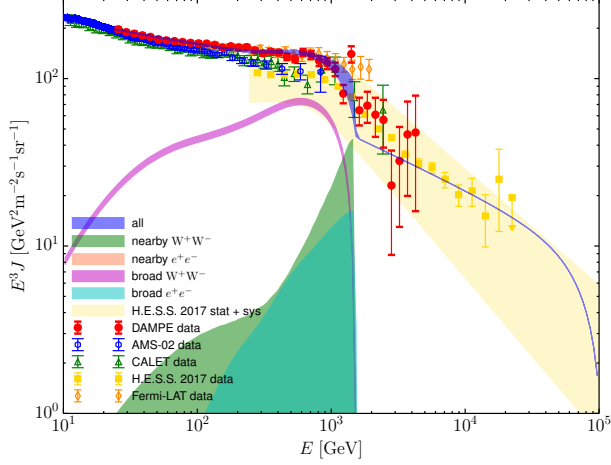


FIG. 12: Same as Fig. 4, but a background consistent with H.E.S.S. 2017 data is adopted. The nearby  $e^+e^-$  component is not seen because it is too weak that is below the x-axis.

the Galactic halo diffuse dark matter contribution could produce the broad process, the result is shown on Fig. 13.

We see that for a reasonable distance of 0.1 kpc, the required halo mass is about  $10^{4.5} M_\odot$ . Using longer dark matter particle lifetime, for example  $\sim 10^{28}$  s, we would have subhalo mass as high as  $10^{6.5} M_\odot$  at 0.1 kpc.

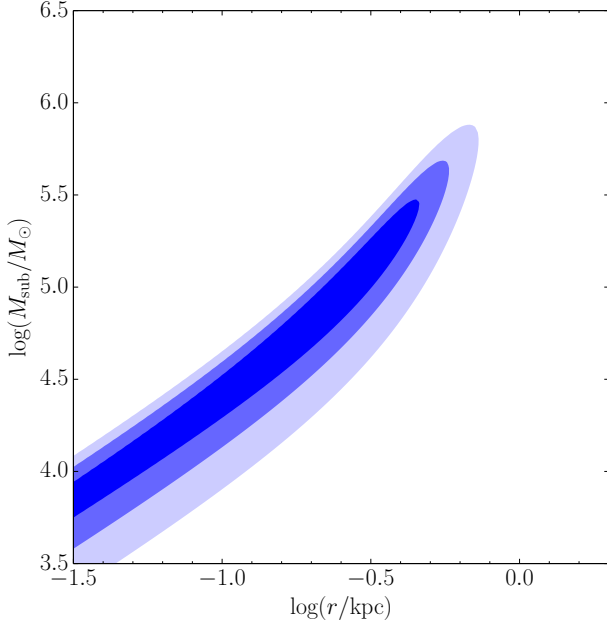


FIG. 13: The constraints on the  $\log(r) - \log(M_{\text{sub}})$  by fitting only the peak for decaying dark matter.

## B. Annihilating dark matter subhalo

For dark matter annihilation, the density profile of the subhalo is crucial. For the subhalo, we assume a power-law density profile (e.g. [81–83])

$$\rho(r) = \rho_0 r^{-\alpha}, \quad M_{\text{sub}} = \frac{4\pi\rho_0}{3-\alpha} r_t^{3-\alpha}, \quad (20)$$

where  $r_t$  is the tidal radius, and

$$\rho_0 = \frac{(3-\alpha)M_{\text{sub}}}{4\pi r_t^{3-\alpha}} \quad (21)$$

The inner cutoff radius for cuspy halo is determined by equating the annihilation time scale to dynamical time scale,  $\tau_d = \tau_{\text{anni}}$ , where

$$\tau_d = \frac{r_t}{\sqrt{GM_{\text{sub}}/r_t}}, \quad \tau_{\text{anni}} = \frac{n_\chi(r_c)}{\dot{n}_\chi(r_c)}. \quad (22)$$

Finally the injection rate from the annihilating dark matter in the subhalo is given by

$$Q_{\text{anni}} = \int_{r_c}^{r_t} 2 \left( \frac{\rho_0 c^2}{E_0} r^{-\alpha} \right)^2 \langle \sigma v \rangle 4\pi r^2 dr \quad (23)$$

$$= \begin{cases} 8\pi \left( \frac{\rho_0 c^2}{E_0} \right)^2 \langle \sigma v \rangle \frac{(r_t^{3-2\alpha} - r_c^{3-2\alpha})}{3-2\alpha} & \text{when } \alpha \neq 1.5 \\ 8\pi \left( \frac{\rho_0 c^2}{E_0} \right)^2 \langle \sigma v \rangle [\ln(r_t) - \ln(r_c)] & \text{when } \alpha = 1.5. \end{cases}$$

For annihilation we assume  $\langle \sigma v \rangle = 10^{-23} \text{ cm}^3 \text{ s}^{-1}$ , for which the annihilation of the diffuse dark matter in Galactic halo gives the broad excess. Then, if the peak is due to the subhalo, the mass and distance of the subhalo is shown in Fig. 14. To fit the peak, assuming the subhalo is located at  $\sim 0.1$  kpc from the Solar system, the required subhalo mass is  $\sim 10^5 M_\odot$  for  $\alpha = 1.2$ . If the halo has a steeper profile, e.g.  $\alpha = 1.7$ , then the halo mass could be as small as  $\sim 10^{2.5} M_\odot$ . A smaller subhalo with very steep density profile could be formed from the large density perturbation peaks ( $\delta\rho/\rho \sim 0.3$ ) in the early Universe in some scenarios (e.g. [84–86].) If we instead adopt a thermal cross-section,  $\langle \sigma v \rangle = 3 \times 10^{-26} \text{ cm}^3 \text{ s}^{-1}$ , we then have that at 0.1 kpc, the required subhalo mass is  $\sim 10^{7.5} M_\odot$  for  $\alpha = 1.2$  and  $\sim 10^{4.5} M_\odot$  for  $\alpha = 1.7$  respectively.

For both the decay and the annihilation models, we obtain the upper limit  $r < 0.53$  kpc ( $3\sigma$  confidence level) after marginalizing the parameter  $Q$ . The constraint is mainly due to achieve the narrow peak with width less than  $\sim 0.2$  TeV.

## C. Inverse Compton Scattering

If such a subhalo is located near the Solar system, it might also produce strong  $\gamma$ -ray photons. Even if we conservatively assume that photons are not produced in the

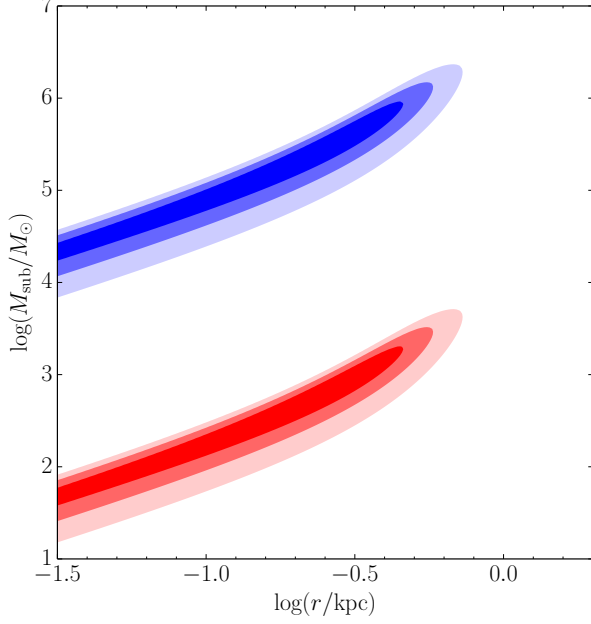


FIG. 14: The constraints on the  $\log(r)$  -  $\log(M_{\text{sub}})$  for dark matter annihilation case,  $\langle\sigma v\rangle = 10^{-23} \text{ cm}^3 \text{ s}^{-1}$  is assumed. The blue contours for  $\alpha = 1.2$ , red for  $\alpha = 1.7$ .

decay or annihilation, the electrons and positrons produced by the subhalo would have ICS with background photons. If a subhalo is a strong electrons/positrons source, it is also a strong ICS source. This would help to identify the subhalo by looking for nearby bright and somewhat extended gamma-ray sources.

Analogously to Eq. (12), we obtain the following emissivity for the up scattered photons:

$$\epsilon(\mathcal{E}, E_0, Q, r) \approx \frac{1}{4\pi} \int dE\psi \sum_i \frac{3\sigma_T c U_{\text{rad},i}}{4\gamma^2 \mathcal{E}_{0,i}^2} G(q_i, \Gamma_{e,i}), \quad (24)$$

where the electron spectrum  $\psi$  is from Eq. 15.

If the line-of-sight is  $\theta$  offset from the center of the subhalo, we have the specific intensity of photons up scattered by electrons generated from a source with  $Q$  injection rate and distance  $r$  from the observer,

$$I_\theta(\mathcal{E}, E_0, Q, r, \theta) = \int_0^\infty \epsilon(\mathcal{E}, E_0, Q, x') dr', \quad (25)$$

where  $x' = \sqrt{r^2 + r'^2 - 2rr'\cos\theta}$ .

We show the ICS specific intensity at 30 GeV for line-of-sight toward the center of the subhalo in Fig. 15. It is much smaller than the isotropic gamma radiation background (IGRB) given in [87]. The expected flux increases with decreasing distance, this is because to achieve the DAMPE peak, the more nearby source needs to produce fewer number of electrons, hence also generating less ICS

radiation. It is still challenge to observe such an extended gamma-ray source by existing or even upcoming instruments.

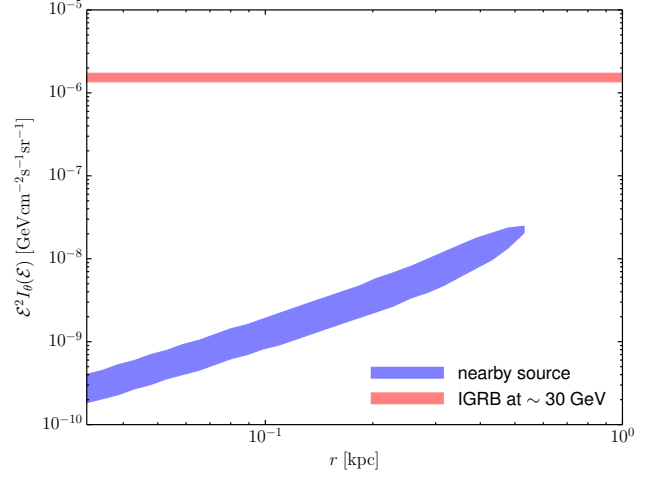


FIG. 15: The predicted gamma-ray intensity at 30 GeV for a subhalo with electrons/positrons that fits the peak (with  $1\sigma$  C.L.), for line-of-sight toward the subhalo center. In the panel we also plot the IGRB given by paper [87].

#### D. Anisotropy

Finally, we note that if the nearby subhalo is involved, it may generate a large anisotropy in the CR flux. This anisotropy, if measured, would be crucial for testing this subhalo scenario, or any similar nearby source scenarios for the CR origins. Currently the anisotropy of the DAMPE  $\sim 1.4$  TeV peak is not analyzed, probably due to the limited particle number: there are only 93 particles detected in the energy bin between 1.3 - 1.5 TeV. Here we present the theoretical quantitative relation between the dipole anisotropy and the distance  $r$ . When the anisotropy analysis released in future, a fast check of the nearby scenario would be possible.

The amplitude of the dipole anisotropy is [88]

$$\left(\frac{\delta J}{J}\right)_{\text{max}} \sim \frac{3D_{xx}}{c\psi} \left|\frac{d\psi}{dr}\right|. \quad (26)$$

In Fig. 16 we show the predicted averaged dipole of electrons/positrons in the energy bin 1.3 - 1.5 TeV, from nearby source that fits the peak. Indeed, if the dipole is measured in future, it would be very helpful for identifying the distance of the nearby source. Obviously, if a dipole  $\lesssim 0.03$  is measured, then it would be in conflict with the requirement by peak width, see Fig. 13 and 14, then the nearby source scenario would be ruled out. On the other hand, if a rather high dipole is measured, then it infers that the source is quite close to us. In this case

the gravity effects of such a subhalo should be carefully inspected.

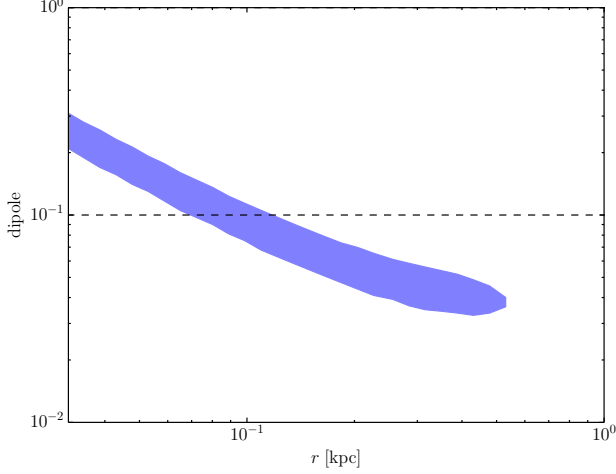


FIG. 16: The predicted dipole from a nearby source at various distance  $r$ . We show the range corresponding the  $1\sigma$  C.L. fits of the peak. To guide the eye we plot the dipole = 0.1 by horizon line.

### E. The probability for the existence of a nearby subhalo

In this subsection we discuss the probability that our Solar system is occasionally close to a subhalo. There have been many simulations that investigate the properties of subhalos in Milky Way-size halos and galaxy clusters (e.g. [89–97]), including the mass function and spatial distribution. Basically, it is found that the mass function is a power-law form.

For example, in the *Aquarius* project [89], for a host halo with mass  $1.839 \times 10^{12} M_\odot$  (Milky Way-size), the mass distribution of subhalos within  $r_{50} = 433.48$  kpc follows the expression

$$\frac{dN_{\text{sub}}}{dM_{\text{sub}}} = a_0 \left( \frac{M_{\text{sub}}}{m_0} \right)^n, \quad (27)$$

where  $a_0 = 3.26 \times 10^{-5} M_\odot^{-1}$ ,  $m_0 = 2.52 \times 10^7 M_\odot$  and  $n = -1.9$ <sup>4</sup>. Moreover, the spatial distribution of their number density is well described by Einasto profile and

<sup>4</sup> The simulations give this relation for subhalos above  $10^5 M_\odot$ , because of the limited resolution, we however extrapolate it down to  $10^3 M_\odot$  in this paper.

is independent of the subhalo mass. It writes

$$\frac{dn_{\text{sub}}}{dM_{\text{sub}}}(M_{\text{sub}}, r) = a_0 \left( \frac{M_{\text{sub}}}{m_0} \right)^n \times A_{\text{sub}} \exp \left( -\frac{2}{\alpha} \left[ \left( \frac{r}{r_{-2}} \right)^\alpha - 1 \right] \right), \quad (28)$$

where  $\alpha = 0.678$  and  $r_{-2} = 199$  kpc, and  $A_{\text{sub}}$  is a normalization factor derived by requiring

$$\int_0^{r_{50}} dr 4\pi r^2 A_{\text{sub}} \exp \left( -\frac{2}{\alpha} \left[ \left( \frac{r}{r_{-2}} \right)^\alpha - 1 \right] \right) = 1. \quad (29)$$

We assume the spatial distribution of subhalos is spherical symmetry, then generate Monte Carlo samples of Milky Way-size halos whose subhalos following the Eq. (28). Then randomly assign the location of our Solar system at the distance 8.5 kpc from the center of the halo. We then count the probability for the existence of a subhalo within different distance  $r$ . The results are shown in Fig. 17.

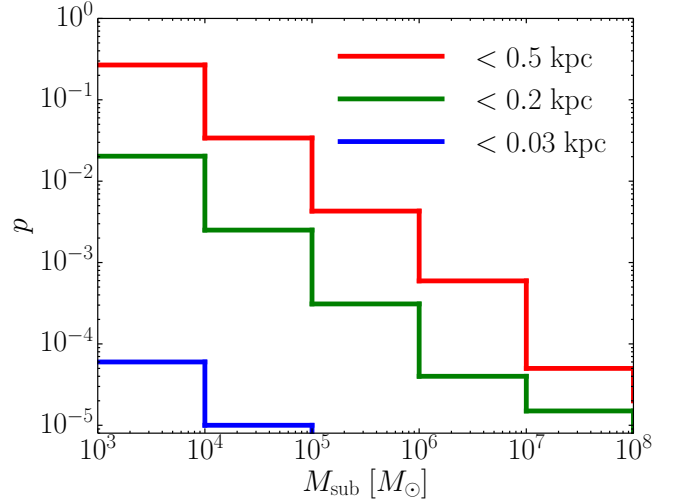


FIG. 17: The probability that our Solar system is occasionally close to a subhalo (within distance  $r$ ) with mass between  $M_{\text{sub}}$  and  $10 \times M_{\text{sub}}$ .

Indeed, the probability that our Solar system is occasionally close to a subhalo is rather small. For example, the probability that a subhalo with mass between  $10^5$  and  $10^6 M_\odot$  within 0.5 kpc is less than 1%. It challenges the subhalo scenario for interpreting the CR excess. This is the problem faced by all similar scenarios and actually has already been noticed long ago (e.g. [98]). For this reason, when we obtain the constraints on subhalo mass and distance, we do not consider this probability.

In our paper, considering the above effect, together with the assumption of enhanced dark matter annihilation cross-section of the order of  $10^{-23} \text{ cm}^3 \text{ s}^{-1}$  and steep density profile with slope  $\alpha \sim -1.7$ , the marginally acceptable parameters (with probability  $\sim 30\%$ ) for subhalo mass and distance are: subhalos with mass  $\sim 10^3 - 10^4 M_\odot$  at distance  $\sim 0.5$  kpc.



## VI. SUMMARY

We studied the CR electron and positron spectrum from dark matter annihilation or decay in the energy range of the recent DAMPE measurement. We obtained the broad excess in the spectrum from a few tens GeV to about 2 TeV, by subtracting the astrophysical background derived from AMS-02  $e^- - e^+$  data and the CR propagation model. We found that for both the  $W^+W^-$  channel and the combination of direct  $e^+e^-$  and double  $\tau^+\tau^-$  channels, diffuse dark matter annihilation or decay in the Galactic halo can provide good fits to the broad excess in the electron and positron spectrum, at least at  $\gtrsim 100$  GeV. This naturally explains the TeV break found in the CR electron and positron spectrum. However, this requires a cross-section of order of  $10^{-23} \text{ cm}^3 \text{ s}^{-1}$ , which is larger than the WIMP cross-section required for obtaining the correct dark matter abundance through thermal decoupling in the early Universe.

In the DAMPE spectrum, there is also a prominent single point peak at  $\sim 1.4$  TeV. Tentatively treating it as real, we investigated how such a peak could be produced, in spite of the energy loss while the electrons and positrons diffusing through the interstellar space. We considered the possibility that the peak is produced by a nearby dark matter subhalo. We found that in the global fit models, there is no peak in the spectrum, and inclusion of the nearby subhalo does not significantly improve the fit. This is because to match the shape of broad spectrum, a suppressed contribution from the direct  $e^+e^-$  channel is favored by the data. As a result, a nearby subhalo is hard to generate a narrow peak, as spectrum of electrons and positrons generated by other channels are always broad.

We then relaxed the requirement of fitting the whole spectrum data, and studied how a spectrum with a  $\sim 1.4$  TeV peak could be generated. We found that in the case of  $W^+W^-$  channel, a peak feature with gentle slope on the low energy side and steep slope on the high energy side can be produced. In the case of double  $\tau^+\tau^-$  channel and direct  $e^+e^-$  channel, a sharp peak feature as found in the DAMPE data could be produced. However, in these cases, the fitting to the broad excess from a few tens to a few hundred GeVs are not very good. In these fits, however, we have assumed a background derived from the AMS-02 experiment. If we rescaled this background, a better fit can be obtained for the dou-

ble  $\tau^+\tau^-$  and direct  $e^+e^-$  channels, even with a peak. Moreover, if we adopted a background spectrum that is consistent with the H.E.S.S. 2017 data when extending to  $\gtrsim 5$  TeV, the conclusions will not change except that a bit higher cross-section is required. These show that the precisely measured spectral shape from DAMPE could provide stringent constraint on the model, though theoretical uncertainty is a very important factor in making interpretation and obtaining the constraint.

Giving the peak strength, we estimated the mass and distance of the subhalo. We found that if assuming this is also the source for broad excess, the required mass for a subhalo 0.1 kpc from our Solar system is  $\sim 10^{4.5} M_\odot$  for the decay case, and  $\sim 10^5 M_\odot$  ( $10^{2.5} M_\odot$ ) for the annihilation case with density profile slope  $\alpha = 1.2$  (1.7). The mass could be even smaller for steeper slope. However, after inspecting the radial distribution of subhalos in a dark matter halo with mass close to our Milky Way's host halo, we found that the probability that a subhalo with mass in above range happens to locate near the Solar system is very small.

We also considered the inverse Compton scattering by the electrons, and the anisotropy in CR if the subhalo is too close by. The inverse Compton scattering radiation is still not observable for current  $\gamma$ -ray telescopes.

**Postscript:** While we were preparing the draft of this paper, we noted that a paper on the theoretical interpretation of the DAMPE result by Q. Yuan et al. [99] appeared on the arxiv preprint server, which investigated both dark matter and pulsar origin of the DAMPE excess and 1.4 TeV peak, though the adopted dark matter models and the methods are somewhat different from ours.

## Acknowledgments

We thank Prof. Jin Chang and Dr. Xiaoyuan Huang for helpful discussions. XLC acknowledges the support of the NSFC through grant No. 1633004 and 11373030, the MoST through grant 2016YFE0100300, and the CAS Frontier Science Key Project No. QYZDJ-SSW-SLH017. BY acknowledges the support of NSFC grant 11653003 and the Bairen program from the Chinese Academy of Sciences (CAS). BY and HBJ acknowledge the support of the NSFC-CAS joint fund for space scientific satellites No. U1738125.

- 
- [1] Planck Collaboration, P. A. R. Ade, N. Aghanim, M. Arnaud, M. Ashdown, J. Aumont, C. Baccigalupi, A. J. Banday, R. B. Barreiro, J. G. Bartlett, et al., *A&A* **594**, A13 (2016), 1502.01589.
  - [2] M. Battaglieri, A. Belloni, A. Chou, P. Cushman, B. Echenard, R. Essig, J. Estrada, J. L. Feng, B. Flaugher, P. J. Fox, et al., *ArXiv e-prints* (2017), 1707.04591.

- [3] A. W. Strong, I. V. Moskalenko, and V. S. Ptuskin, *Annual Review of Nuclear and Particle Science* **57**, 285 (2007), astro-ph/0701517.
- [4] M. A. DuVernois, S. W. Barwick, J. J. Beatty, A. Bhatlacharyya, C. R. Bower, C. J. Chaput, S. Coutu, G. A. de Nolfo, D. M. Lowder, S. McKee, et al., *ApJ* **559**, 296 (2001).
- [5] J. Chang, J. H. Adams, H. S. Ahn, G. L.

- Bashindzhagyan, M. Christl, O. Ganel, T. G. Guzik, J. Isbert, K. C. Kim, E. N. Kuznetsov, et al., *Nature* **456**, 362 (2008).
- [6] O. Adriani, G. C. Barbarino, G. A. Bazilevskaya, R. Bellotti, M. Boezio, E. A. Bogomolov, M. Bongi, V. Bonvicini, S. Borisov, S. Bottai, et al., *Physical Review Letters* **106**, 201101 (2011), 1103.2880.
- [7] A. A. Abdo, M. Ackermann, M. Ajello, W. B. Atwood, M. Axelsson, L. Baldini, J. Ballet, G. Barbiellini, D. Bastieri, M. Battelino, et al., *Physical Review Letters* **102**, 181101 (2009), 0905.0025.
- [8] S. Abdollahi, M. Ackermann, M. Ajello, W. B. Atwood, L. Baldini, G. Barbiellini, D. Bastieri, R. Bellazzini, E. D. Bloom, R. Bonino, et al., *Phys. Rev. D* **95**, 082007 (2017).
- [9] M. Aguilar, D. Aisa, B. Alpat, A. Alvino, G. Ambrosi, K. Andeen, L. Arruda, N. Attig, P. Azzarello, A. Bachlechner, et al., *Physical Review Letters* **113**, 221102 (2014).
- [10] A. Abramowski, F. Acero, F. Aharonian, A. G. Akhperjanian, G. Anton, A. Barnacka, U. Barres de Almeida, A. R. Bazer-Bachi, Y. Becherini, J. Becker, et al., *Physical Review Letters* **106**, 161301 (2011), 1103.3266.
- [11] F. Aharonian, A. G. Akhperjanian, U. Barres de Almeida, A. R. Bazer-Bachi, Y. Becherini, B. Behera, W. Benbow, K. Bernlöhner, C. Boisson, A. Bochow, et al., *Physical Review Letters* **101**, 261104 (2008), 0811.3894.
- [12] F. Aharonian, A. G. Akhperjanian, G. Anton, U. Barres de Almeida, A. R. Bazer-Bachi, Y. Becherini, B. Behera, K. Bernlöhner, A. Bochow, C. Boisson, et al., *A&A* **508**, 561 (2009), 0905.0105.
- [13] M. Cirelli, M. Kadastik, M. Raidal, and A. Strumia, *Nuclear Physics B* **813**, 1 (2009), 0809.2409.
- [14] P. S. B. Dev, D. K. Ghosh, N. Okada, and I. Saha, *Phys. Rev. D* **89**, 095001 (2014), 1307.6204.
- [15] S. Profumo, F. S. Queiroz, J. Silk, and C. Siqueira, *ArXiv e-prints* (2017), 1711.03133.
- [16] L. Bergström, J. Edsjö, and G. Zaharijas, *Physical Review Letters* **103**, 031103 (2009), 0905.0333.
- [17] J. L. Feng, M. Kaplinghat, and H.-B. Yu, *Phys. Rev. D* **82**, 083525 (2010), 1005.4678.
- [18] G. Zaharijas, A. Cuoco, Z. Yang, J. Conrad, and for the Fermi-LAT collaboration, *ArXiv e-prints* (2010), 1012.0588.
- [19] Y. Zhao, X.-J. Bi, H.-Y. Jia, P.-F. Yin, and F.-R. Zhu, *Phys. Rev. D* **93**, 083513 (2016), 1601.02181.
- [20] W. Liu, X.-J. Bi, S.-J. Lin, B.-B. Wang, and P.-F. Yin, *Phys. Rev. D* **96**, 023006 (2017), 1611.09118.
- [21] B.-Q. Lu, Y.-L. Wu, W.-H. Zhang, and Y.-F. Zhou, *ArXiv e-prints* (2017), 1711.00749.
- [22] Y. Zhao, X.-J. Bi, P.-F. Yin, and X. Zhang, *ArXiv e-prints* (2017), 1711.04696.
- [23] S.-J. Lin, Q. Yuan, and X.-J. Bi, *Phys. Rev. D* **91**, 063508 (2015), 1409.6248.
- [24] D. Malyshev, I. Cholis, and J. Gelfand, *Phys. Rev. D* **80**, 063005 (2009), 0903.1310.
- [25] H.-B. Hu, Q. Yuan, B. Wang, C. Fan, J.-L. Zhang, and X.-J. Bi, *ApJ* **700**, L170 (2009), 0901.1520.
- [26] I. Cholis and D. Hooper, *Phys. Rev. D* **88**, 023013 (2013), 1304.1840.
- [27] R. Blandford, P. Simeon, and Y. Yuan, *Nuclear Physics B Proceedings Supplements* **256**, 9 (2014), 1409.2589.
- [28] Y. Fujita, K. Kohri, R. Yamazaki, and K. Ioka, *Phys. Rev. D* **80**, 063003 (2009), 0903.5298.
- [29] K. Kohri, K. Ioka, Y. Fujita, and R. Yamazaki, *Progress of Theoretical and Experimental Physics* **2016**, 021E01 (2016), 1505.01236.
- [30] P. Blasi and P. D. Serpico, *Physical Review Letters* **103**, 081103 (2009), 0904.0871.
- [31] P. Blasi, *Physical Review Letters* **103**, 051104 (2009), 0903.2794.
- [32] P. D. Serpico, *Astroparticle Physics* **39**, 2 (2012), 1108.4827.
- [33] P. Mertsch and S. Sarkar, *Physical Review Letters* **103**, 081104 (2009), 0905.3152.
- [34] P. Mertsch and S. Sarkar, *Physical Review Letters* **107**, 091101 (2011), 1104.3585.
- [35] D. Donato, S. B. Cenko, S. Covino, E. Troja, T. Purumo, C. C. Cheung, O. Fox, A. Kuttyrev, S. Campana, D. Fugazza, et al., *ApJ* **781**, 59 (2014), 1311.6162.
- [36] P. Mertsch and S. Sarkar, *Phys. Rev. D* **90**, 061301 (2014), 1402.0855.
- [37] N. Tomassetti and F. Donato, *A&A* **544**, A16 (2012), 1203.6094.
- [38] N. Tomassetti and F. Donato, *ApJ* **803**, L15 (2015), 1502.06150.
- [39] J. Chang, G. Ambrosi, Q. An, R. Asfandiyarov, P. Azzarello, P. Bernardini, B. Bertucci, M. S. Cai, M. Caragiulo, D. Y. Chen, et al., *Astroparticle Physics* **95**, 6 (2017), 1706.08453.
- [40] DAMPE collaboration, *Nature* **551** (2017), arxiv:1711.10981.
- [41] F.-L. Collaboration, :, S. Abdollahi, M. Ackermann, M. Ajello, W. B. Atwood, L. Baldini, G. Barbiellini, D. Bastieri, R. Bellazzini, et al., *Physical Review D* **95**, 082007 (2017), ISSN 2470-0010, 1704.07195.
- [42] O. Adriani, Y. Akaike, K. Asano, Y. Asaoka, M. G. Bagliesi, G. Bigongiari, W. R. Binns, S. Bonechi, M. Bongi, P. Brogi, et al., *Physical Review Letters* **119**, 181101 (2017), 1712.01711.
- [43] V. S. Berezhinskii, S. V. Bulanov, V. A. Dogiel, and V. L. Ginzburg, *Astrophysics of cosmic rays* (North-Holland, Amsterdam, 1990), ISBN 0444886419.
- [44] A. W. Strong and I. V. Moskalenko, *The Astrophysical Journal* **509**, 212 (1998), ISSN 0004-637X, 9807150.
- [45] R. Blandford and D. Eichler, *Physics Reports* **154**, 1 (1987), ISSN 03701573.
- [46] A. E. Vladimirov, S. W. Digel, G. Jóhannesson, P. F. Michelson, I. V. Moskalenko, P. L. Nolan, E. Orlando, T. A. Porter, and A. W. Strong, *Computer Physics Communications* **182**, 1156 (2011), 1008.3642.
- [47] I. V. Moskalenko, A. W. Strong, J. F. Ormes, and M. S. Potgieter, *The Astrophysical Journal* **565**, 280 (2001), ISSN 0004-637X, 0106567.
- [48] A. Strong and J. Mattox, *Astron. Astrophys.* **308**, L21 (1996).
- [49] M. Aguilar, D. Aisa, B. Alpat, A. Alvino, G. Ambrosi, K. Andeen, L. Arruda, N. Attig, P. Azzarello, A. Bachlechner, et al., *Physical Review Letters* **114**, 171103 (2015), ISSN 0031-9007.
- [50] M. Aguilar, L. Ali Cavazonza, G. Ambrosi, L. Arruda, N. Attig, S. Aupetit, P. Azzarello, A. Bachlechner, F. Barao, A. Barrau, et al., *Physical Review Letters* **117**, 231102 (2016), ISSN 0031-9007.
- [51] H.-B. Jin, Y.-L. Wu, and Y.-F. Zhou, *Journal of Cosmology and Astroparticle Physics* **2015**, 049 (2015), ISSN 1475-7516, 1410.0171.
- [52] J. F. Navarro, C. S. Frenk, and S. D. M. White, *The*



- Astrophysical Journal **490**, 493 (1996), ISSN 0004-637X, 9611107.
- [53] L. Bergstrom, P. Ullio, and J. Buckley, *Astroparticle Physics* **9**, 44 (1997), ISSN 09276505, 9712318.
  - [54] B. Moore, S. Ghigna, F. Governato, G. Lake, T. Quinn, J. Stadel, and P. Tozzi, *The Astrophysical Journal* **524**, 4 (1999), ISSN 0004637X, 9907411.
  - [55] J. Einasto, in *Astronomy and Astrophysics 2010* (2009), p. 31, 0901.0632.
  - [56] T. Sjöstrand, S. Mrenna, and P. Skands, *Computer Physics Communications* **178**, 852 (2008), ISSN 00104655, 0710.3820.
  - [57] H.-B. Jin, Y.-L. Wu, and Y.-F. Zhou (2017), 1701.02213.
  - [58] M. Aguilar, D. Aisa, A. Alvino, G. Ambrosi, K. Andeen, L. Arruda, N. Attig, P. Azzarello, A. Bachlechner, F. Barao, et al., *Physical Review Letters* **113**, 121102 (2014), ISSN 0031-9007.
  - [59] L. Accardo, M. Aguilar, D. Aisa, B. Alpat, A. Alvino, G. Ambrosi, K. Andeen, L. Arruda, N. Attig, P. Azzarello, et al., *Physical Review Letters* **113**, 121101 (2014), ISSN 0031-9007.
  - [60] H.-B. Jin, Y.-L. Wu, and Y.-F. Zhou, *Journal of Cosmology and Astroparticle Physics* **2013**, 026 (2013), ISSN 1475-7516, 1304.1997.
  - [61] Z.-P. Liu, Y.-L. Wu, and Y.-F. Zhou, *Physical Review D* **88**, 096008 (2013), ISSN 1550-7998, 1305.5438.
  - [62] J. Chen, Z.-L. Liang, Y.-L. Wu, and Y.-F. Zhou, *Journal of Cosmology and Astroparticle Physics* **2015**, 021 (2015), ISSN 1475-7516, 1505.04031.
  - [63] Y.-F. Zhou, *PoS DSU2015*, 22 (2016).
  - [64] D. Chen, J. Huang, and H.-B. Jin, *The Astrophysical Journal* **811**, 154 (2015), ISSN 1538-4357, 1412.2499.
  - [65] P. Salucci, F. Nesti, G. Gentile, and C. F. Martins, *Astronomy & Astrophysics* **523**, 6 (2010), ISSN 0004-6361, 1003.3101.
  - [66] A. W. Strong, I. V. Moskalenko, and O. Reimer, *The Astrophysical Journal* **537**, 763 (2000), ISSN 0004-637X, 9811296.
  - [67] B. Moore, S. Ghigna, F. Governato, G. Lake, T. Quinn, J. Stadel, and P. Tozzi, *ApJ* **524**, L19 (1999), astro-ph/9907411.
  - [68] A. Klypin, A. V. Kravtsov, O. Valenzuela, and F. Prada, *ApJ* **522**, 82 (1999), astro-ph/9901240.
  - [69] J. S. Bullock and M. Boylan-Kolchin, *ARA&A* **55**, 343 (2017), 1707.04256.
  - [70] R. Trotta, G. Jóhannesson, I. V. Moskalenko, T. A. Porter, R. Ruiz de Austri, and A. W. Strong, *ApJ* **729**, 106 (2011), 1011.0037.
  - [71] M. Haverkorn, in *Magnetic Fields in Diffuse Media*, edited by A. Lazarian, E. M. de Gouveia Dal Pino, and C. Melioli (2015), vol. 407 of *Astrophysics and Space Science Library*, p. 483, 1406.0283.
  - [72] E. Lefa, S. R. Kelner, and F. A. Aharonian, *ApJ* **753**, 176 (2012), 1205.2929.
  - [73] T. A. Porter and A. W. Strong, *International Cosmic Ray Conference* **4**, 77 (2005), astro-ph/0507119.
  - [74] T. A. Porter, I. V. Moskalenko, and A. W. Strong, *ApJ* **648**, L29 (2006), astro-ph/0607344.
  - [75] D. Staszak and f. t. V. Collaboration, in *Proceedings, 34th International Cosmic Ray Conference (ICRC 2015)* (2015), 1508.06597.
  - [76] F. Aharonian et al. (H.E.S.S.), *Phys. Rev. Lett.* **101**, 261104 (2008), 0811.3894.
  - [77] F. Aharonian et al. (H.E.S.S.), *Astron. Astrophys.* **508**, 561 (2009), 0905.0105.
  - [78] M. Ackermann, M. Ajello, W. B. Atwood, L. Baldini, J. Ballet, G. Barbiellini, D. Bastieri, B. M. Baughman, K. Bechtol, F. Bellardi, et al., *Physical Review D* **82**, 092004 (2010), ISSN 1550-7998, 1008.3999.
  - [79] VERITAS Collaboration, S. Archambault, A. Archer, W. Benbow, R. Bird, E. Bourbeau, T. Brantseg, M. Buchovecky, J. H. Buckley, V. Bugaev, et al., *Physical Review D* **95**, 082001 (2017), ISSN 2470-0010, 1703.04937.
  - [80] F.-L. Collaboration, *Physical Review Letters* **115**, 231301 (2015), ISSN 0031-9007, 1503.02641.
  - [81] D. Reed, F. Governato, L. Verde, J. Gardner, T. Quinn, J. Stadel, D. Merritt, and G. Lake, *MNRAS* **357**, 82 (2005), astro-ph/0312544.
  - [82] J. Diemand, M. Kuhlen, and P. Madau, *ApJ* **649**, 1 (2006), astro-ph/0603250.
  - [83] D. Hooper and S. J. Witte, *J. Cosmology Astropart. Phys.* **4**, 018 (2017), 1610.07587.
  - [84] Y. Yang, *European Physical Journal Plus* **131**, 432 (2016), 1612.06559.
  - [85] Y. Yang, G. Yang, X. Huang, X. Chen, T. Lu, and H. Zong, *Phys. Rev. D* **87**, 083519 (2013), 1206.3750.
  - [86] Y. Yang, G. Yang, and H. Zong, *Phys. Rev. D* **87**, 103525 (2013), 1305.4213.
  - [87] M. Ackermann, M. Ajello, A. Albert, W. B. Atwood, L. Baldini, J. Ballet, G. Barbiellini, D. Bastieri, K. Bechtol, R. Bellazzini, et al., *The Astrophysical Journal* **799**, 86 (2015), ISSN 1538-4357, 1410.3696.
  - [88] N. Globus and T. Piran, *ApJ* **850**, L25 (2017), 1709.10110.
  - [89] V. Springel, J. Wang, M. Vogelsberger, A. Ludlow, A. Jenkins, A. Helmi, J. F. Navarro, C. S. Frenk, and S. D. M. White, *MNRAS* **391**, 1685 (2008), 0809.0898.
  - [90] J. Diemand, M. Kuhlen, and P. Madau, *ApJ* **657**, 262 (2007), astro-ph/0611370.
  - [91] J. Diemand, M. Kuhlen, and P. Madau, *ApJ* **667**, 859 (2007), astro-ph/0703337.
  - [92] J. Diemand, M. Kuhlen, P. Madau, M. Zemp, B. Moore, D. Potter, and J. Stadel, *Nature* **454**, 735 (2008), 0805.1244.
  - [93] L. Gao, C. S. Frenk, M. Boylan-Kolchin, A. Jenkins, V. Springel, and S. D. M. White, *MNRAS* **410**, 2309 (2011), 1006.2882.
  - [94] L. Gao, J. F. Navarro, C. S. Frenk, A. Jenkins, V. Springel, and S. D. M. White, *MNRAS* **425**, 2169 (2012), 1201.1940.
  - [95] F. Jiang and F. C. van den Bosch, *MNRAS* **458**, 2848 (2016).
  - [96] F. C. van den Bosch and F. Jiang, *MNRAS* **458**, 2870 (2016).
  - [97] C. Giocoli, G. Tormen, and F. C. van den Bosch, *MNRAS* **386**, 2135 (2008), 0712.1563.
  - [98] P. Brun, T. Delahaye, J. Diemand, S. Profumo, and P. Salati, *Phys. Rev. D* **80**, 035023 (2009), 0904.0812.
  - [99] Q. Yuan, L. Feng, P.-F. Yin, Y.-Z. Fan, X.-J. Bi, M.-Y. Cui, T.-K. Dong, Y.-Q. Guo, K. Fang, H.-B. Hu, et al., *ArXiv e-prints* (2017), 1711.10989.